CHEMISTRY OF MATERIALS

Article

pubs.acs.org/cm

Thieno[3,2-*b*]thiophene-Substituted Benzo[1,2-*b*:4,5-*b*′]dithiophene as a Promising Building Block for Low Bandgap Semiconducting Polymers for High-Performance Single and Tandem Organic Photovoltaic Cells

Ji-Hoon Kim,[†] Chang Eun Song,[‡] BongSoo Kim,[§] In-Nam Kang,[∥] Won Suk Shin,[⊥] and Do-Hoon Hwang*,[†]

[†]Department of Chemistry and Chemistry Institute for Functional Materials, Pusan National University, Busan 609-735, Republic of Korea

[‡]Department of Materials Science and Engineering, KAIST, Daejeon 305-701, Republic of Korea

[§]Photoelectronic Hybrids Research Center, Korea Institute of Science and Technology (KIST), Seoul 136-791, Republic of Korea

[∥]Department of Chemistry, The Catholic University of Korea, Bucheon 420-743, Republic of Korea

[⊥]Energy Materials Research Center, Korea Research Institute of Chemical Technology, Daejeon 305-343, Republic of Korea

Supporting Information

ABSTRACT: We designed and synthetized a new poly{4,8-bis((2-ethylhexyl)-thieno[3,2-*b*]thiophene)-benzo[1,2-*b*:4,5-*b*′]dithiophene-*alt*-2-ethylhexyl-4,6-dibromo-3-fluorothieno[3,4-*b*]thiophene-2-carboxylate} (PTTBDT-FTT) comprising bis(2-ethylhexylthieno[3,2-*b*]thiophenylbenzo[1,2-*b*:4,5-*b*′]dithiophene (TTBDT) and 2-ethylhexyl 3-fluorothieno[3,4-*b*]thiophene-2-carboxylate (FTT). The optical bandgap of PTTBDT-FTT was 1.55 eV. The energy levels of the highest occupied and lowest unoccupied molecular orbitals of PTTBDT-FTT were −5.31 and −3.73 eV, respectively. Two-dimensional grazing-incidence X-ray scattering measurements showed that the film's PTTBDT-FTT chains are predominantly arranged with a face-on orientation with respect to the substrate, with strong $\pi-\pi$ stacking. An organic thin-film transistor fabricated using PTTBDT-FTT as the active semiconductor showed high hole mobility of 2.1 × 10^{-2} $cm^2/(V\cdot s)$. Single-junction bulk heterojunction photovoltaic cells with the configuration ITO/PEDOT:PSS/PTTBDT-FTT:$PC_{71}BM$/Ca/Al were fabricated, which showed a maximum power conversion efficiency (PCE) of 7.44%. Inverted photovoltaic cells with the structure ITO/PEIE/PTTBDT-FTT:$PC_{71}BM$/MoO_3/Ag were also fabricated, with a maximum PCE of 7.71%. A tandem photovoltaic device comprising the inverted PTTBDT-FTT:$PC_{71}BM$ cell and a P3HT:ICBA-based cell as the top and bottom cell components, respectively, showed a maximum PCE of 8.66%. This work demonstrated that the newly developed PTTBDT-FTT polymer was very promising for applications in both single and tandem solar cells. Furthermore, this work highlighted the fact that an extended π-system in the electron-donor moiety in low bandgap polymers is crucial for improving polymer solar cells.

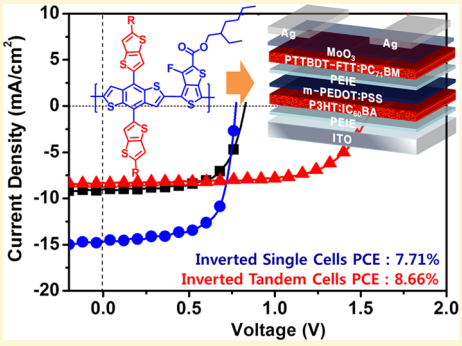

1. INTRODUCTION

The active layer of a bulk heterojunction (BHJ) organic photovoltaic cell (OPV) comprises a blend of p-type conjugated polymers and n-type accepting materials such as fullerene derivatives. Efforts toward developing high power conversion efficiency (PCE) BHJ OPVs include the design and synthesis of new p-type conjugated polymers and n-type accepting materials, use of various additives to tune the morphology of the active layer, optimization of processing techniques, and adoption of new device architectures.[1−6] However, OPVs tend to have low open-circuit voltages (V_{oc}), which limits further PCE improvements. In addition, significant energy losses are unavoidable for single BHJ OPVs because photons with energies lower or higher than the bandgap energy of the BHJ layer are not absorbed and cannot generate electron−hole pairs. Only absorbed photons can be involved in the energy conversion process and the nonabsorbed energy is lost by thermalization. Tandem device architectures have been demonstrated to be a useful approach to the fabrication of high-efficiency photovoltaic cells, where two subcells are stacked in series and the individual photoactive layers have complementary absorption spectra.[7−12] This tandem configuration can address the limitations of single BHJ OPVs as a broader spectrum of solar radiation can be covered by bottom and top cells and thermalization losses can be reduced. Furthermore, a high V_{oc} can be obtained because the V_{oc} of an optimized

Received: November 7, 2013
Revised: December 25, 2013
Published: December 25, 2013

   dx.doi.org/10.1021/cm4035903 | *Chem. Mater.* 2014, 26, 1234−1242

Scheme 1[a]

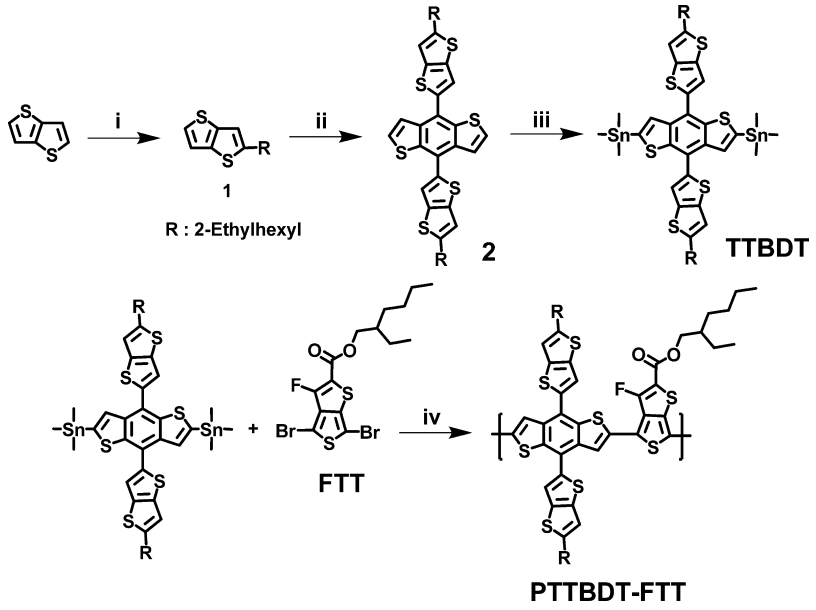

[a]Reagents and Conditions: (i) *n*-BuLi, 2-ethylhexylbromide, THF, −78 °C, 12 h; (ii) *n*-BuLi, 4,8-dehydrobenzo[1,2-b:4,5-b′]dithiophene-4,8-dione, $SnCl_2 \cdot H_2O$, 0 °C, then 50 °C, THF; (iii) TMEDA, *n*-BuLi, $Sn(Me)_3Cl$, −78 °C, THF; (iv) $Pd(PPh_3)_4$, toluene, DMF, 110 °C, 48 h, argon.

tandem cell is the sum of the V_{oc}'s of the individual subcells. According to the simulated results obtained by Dennler et al., a PCE as high as 15% is achievable for a polymer tandem cell with an optimized material combination.[13] PCEs higher than 10% have recently been reported for both polymer tandem cells and vacuum-processed small-molecule tandem cells, showing that the tandem structure provides a promising means of enhancing PCEs.[14−16]

Benzodithiophene (BDT)[17,18] and thieno[3,4-*b*]thiophene (TT)[19] are of particular interest in the synthesis of low bandgap polymers as electron-donating and electron-withdrawing building blocks, respectively, since they offer very high PCEs as a result of their high short-circuit currents (J_{sc}) and V_{oc} values. Alkylthienyl-substituted benzo[1,2-*b*:4,5-*b*′]-dithiophenes (BDTTs), which have two-dimensional conjugated structures, have been used to enhance intermolecular $\pi-\pi$ interactions by extending the conjugated surfaces of BDT-based polymers.[20−22] Consequently, replacement of the alkoxy moiety by an alkylthienyl has been used to improve the photovoltaic properties of BDT-based polymers. Interestingly, according to the reported results, most of the polymers consisting of BDT and TT are amorphous.[23,24] Determining the reason for the amorphous nature of PBDTTT derivatives and developing new molecular designs for improving the crystallinity or $\pi-\pi$ interactions of low bandgap polymers is therefore crucial for fabricating high-performance OPVs.

In this study, we designed and synthesized a thieno[3,2-*b*]thiophene-substituted benzo[1,2-*b*:4,5-*b*′]dithiophene derivative as a new donor building block for donor−acceptor-type low bandgap polymers. Poly{4,8-bis((2-ethylhexyl)thieno[3,2-*b*]thiophene)-benzo[1,2-*b*:4,5-*b*′]dithiophene-*alt*-2-ethylhexyl-4,6-dibromo-3-fluorothieno[3,4-*b*]thiophene-2-carboxylate} (PTTBDT-FTT) was synthesized through Stille cross-coupling, using a 2,6-bis(trimethyltin)-4,8-bis((2-ethylhexyl)thieno[3,2-*b*]thiophene)-benzo[1,2-*b*:4,5-*b*′]dithiophene (TTBDT) and 2-ethylhexyl 4,6-dibromo-3-fluorothieno[3,4-*b*]thiophene-2-carboxylate (FTT) moieties, as shown in Scheme 1. The introduction of thieno[3,2-*b*]thiophene to the BDT unit provided improved π-orbital overlap between conjugated polymer chains, molecular ordering, and hole mobility. The PCEs of the conventional and inverted photovoltaic cells fabricated using PTTBDT-FTT are 7.44% and 7.71%, respectively. Moreover, a PCE of 8.66% was achieved using PTTBDT-FTT as the photoactive component in the top cell of a solution-processed inverted tandem OPV. The synthetic routes and chemical structure of PTTBDT-FTT are shown in Scheme 1.

2. RESULTS AND DISCUSSION

2.1. Synthesis and Characterization of Polymers. PTTBDT-FTT was synthesized by Stille cross-coupling polymerization of TTBDT with FTT in the presence of $Pd(PPh_3)_4$ as a catalyst. The synthesized PTTBDT-FTT showed good solubility in common organic solvents such as chloroform, chlorobenzene, and toluene, and the polymer solution formed uniform thin films by spin-coating. The number-average molecular-weight (M_n) and polydispersity index (PDI) of the PTTBDT-FTT were determined using gel permeation chromatography (GPC) with polystyrene as a standard. The M_n of PTTBDT-FTT was found to be 25 000 g/mol, with a PDI of 2.46 (Supporting Information Figure S1). The thermal stability of the polymer was investigated using thermogravimetric analysis (TGA), which revealed that the 5% weight loss temperature of PTTBDT-FTT was 428 °C (Supporting Information Figure S2). Interestingly, no obvious exothermic and endothermic peaks were found in the temperature range between 25 and 250 °C using differential scanning calorimetry, suggesting that the morphology of a PTTBDT-FTT film would be stable in this temperature range [Supporting Information Figure S2 (inset)].

2.2. Optical and Electrochemical Properties. Figure 1a shows the UV−visible absorption spectra of PTTBDT-FTT in chloroform solution and in the film state. Both spectra show similar profiles, with a peak absorption at around 700 nm

dx.doi.org/10.1021/cm4035903 | *Chem. Mater.* 2014, 26, 1234−1242

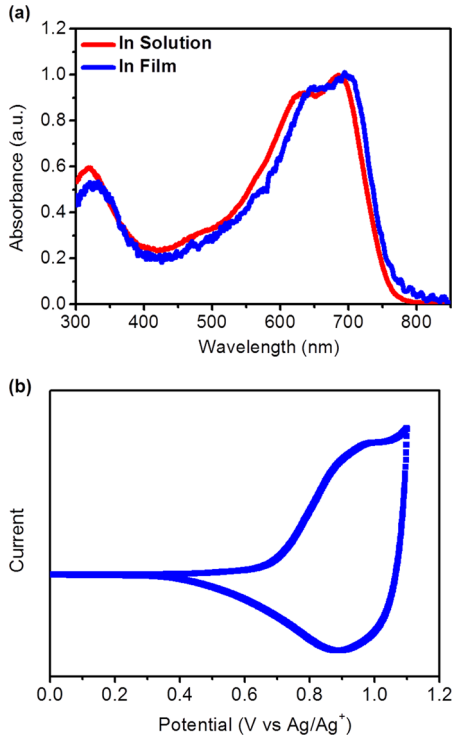

Figure 1. Normalized absorption spectra of PTTBDT-FTT in (a) chloroform solution and in thin films. (b) Cyclic voltammograms of PTTBDT-FTT film on a platinum electrode in 0.10 M $TBABF_4$ acetonitrile solution.

arising from the $\pi-\pi^*$ transitions of the conjugated polymer backbones. The absorption band of PTTBDT-FTT moved slightly to the longer wavelength region compared with that of the polymer solution. The optical bandgap determined form the absorption edge of the PTTBDT-FTT film was 1.55 eV; this is slightly smaller than the value of 1.63 eV for the similarly structured poly({4,8-bis[(2-ethylhexyl)oxy]benzo[1,2-*b*:4,5-*b*′]-dithiophene-2,6-diyl}-*alt*-{3-fluoro-2-[(2-ethylhexyl)carbonyl]-thieno[3,4-*b*]thiophenediyl}) (PTB7), indicating that PTTBDT-FTT has more extended conjugation and/or enhanced interchain $\pi-\pi$ interactions than PTB7 does, as a result of the thieno[3,2-*b*]thiophene units. The measured molar extinction coefficient of the PTTBDT-FTT film at the peak absorption was 1.2×10^5 cm^{-1} at 700 nm, which is higher than those reported for similar semiconducting polymers (Supporting Information Figure S3).[23,24]

The highest occupied molecular orbital (HOMO) and lowest unoccupied molecular orbital (LUMO) energy levels of the PTTBDT-FTT film were determined by cyclic voltammetry (CV), with a Pt plate as the counter electrode and Ag/Ag^+ as the reference electrode in anhydrous acetonitrile (CH_3CN) solution with 0.1 M tetrabutylammonium tetrafluoroborate ($TBABF_4$), at a scan rate of 50 mV/s. A Pt plate coated with a thin film of the PTTBDT-FTT, a Pt wire, and $Ag/AgNO_3$ were used as the work electrode, counter electrode, and reference electrode, respectively. The HOMO energy level of the $Ag/AgNO_3$ reference electrodes was calibrated against the ferrocene/ferrocenium (Fc/Fc^+) system to be 4.70 eV in this work.[25,26] PTTBDT-FTT exhibited one oxidation process (with an onset oxidation potential E_{ox}^{onset} = 0.61 V vs Ag/Ag^+), as shown in Figure 1b. The HOMO energy values were calculated using the equation $E_{HOMO} = -(E_{ox}^{onset} + 4.70)$ eV, where E_{ox}^{onset} is the onset oxidation potential versus Ag/Ag^+. PTTBDT-FTT exhibited a relatively low-lying HOMO energy level of −5.31 eV, which is in the ideal range for ensuring oxidative stability and producing a higher V_{oc}. The LUMO levels of the polymers were determined from the HOMO levels obtained from the CV measurements and the E_g^{opt} values obtained from the UV−visible absorption edges. The measured LUMO energy level of PTTBDT-FTT was −3.76 eV, which is 0.54 eV higher than that of $PC_{71}BM$ (−4.30 eV), suggesting that charge transfer from the polymer to $PC_{71}BM$ would be efficient. The UV−visible absorption properties, E_g^{opt} values, and HOMO/LUMO energy levels of the polymers are summarized in Supporting Information Table S1.

2.3. Two-Dimensional Grazing-Incidence X-ray Scattering (2D-GIXS) and Structural Properties. 2D-GIXS measurements were performed to determine the extent of cofacial π-stacking, crystallinity, and the polymer-packing orientation relative to the substrate. Figure 2 shows the 2D-

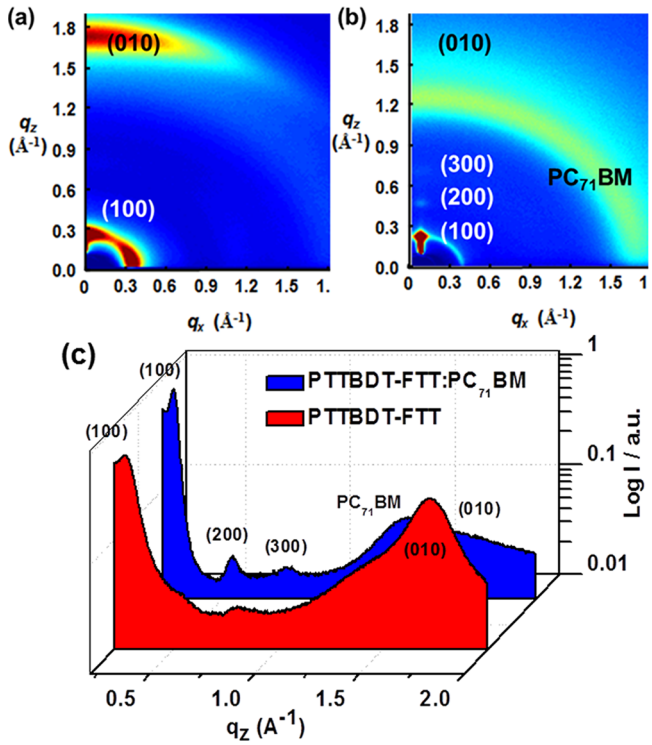

Figure 2. Two-dimensional grazing-incidence wide-angle X-ray scattering (GIXS) pattern of (a) pure PTTBDT-FTT and (b) PTTBDT-FTT:$PC_{71}BM$ films. (c) Out-of-plane of line cut profiles of GIXS images for the pure films of PTTBDT-FTT and the blend of PTTBDT-FTT:$PC_{71}BM$ (1:1.5, w/w).

GIXS images of pure PTTBDT-FTT and PTTBDT-FTT:$PC_{71}BM$ blends. Figure 2a shows the GIXS image of pure the PTTBDT-FTT film. The GIXS pattern of the PTTBDT-FTT film showed intense diffraction peaks at both q_{xy} and q_z (q_z = 0.26 $Å^{-1}$), which correspond to the (100) reflection of the polymer crystal with a lamellar domain spacing (d_1) of 2.46 nm. For the PTTBDT-FTT film, a very strong (010) $\pi-\pi$ stacking peak at around 1.70 $Å^{-1}$ was observed, which corresponds to a d_{010} of 0.40 nm. This is a typical $\pi-\pi$ stacking distance in low bandgap conjugated polymers with good photovoltaic performances.[27,28] It can be concluded that the PTTBDT-FTT polymer chains in the film are predom-

dx.doi.org/10.1021/cm4035903 | *Chem. Mater.* 2014, 26, 1234−1242

inantly arranged with a face-on orientation to the substrate (40−50 nm thick PEDOT:PSS layer on Si wafer). Figure 2b shows the GIXS image of a PTTBDT-FTT:$PC_{71}BM$ (1:2, w/w) blend film. Interestingly, the donor−acceptor blend film showed (100), (200), and (300) peaks with more pronounced reflections, indicating that the polymer stacks in the film have high structural organization. This high structural ordering of the active layer enables high J_{sc} and fill factor (FF) values to be achieved in OPV devices (see below).

To compare the crystal behavior of PTTBDT-FTT with that of PTB7, the same GIXS measurements were performed with a PTB7:$PC_{71}BM$ blend film. The GIXS images are provided in Supporting Information Figure S4. PTB7:$PC_{71}BM$ and PTTBDT-FTT:$PC_{71}BM$ showed similar scattering patterns, but the PTB7:$PC_{71}BM$ film showed lower molecular ordering than PTTBDT-FTT:$PC_{71}BM$ did, as shown by the in-plane and out-of-plane scattering profiles. PTTBDT-FTT therefore showed good molecular ordering, even in the polymer:$PC_{71}BM$ blend film, compared with PTB7.

2.4. Organic Thin-Film Transistor (OTFT) Characteristics of Polymer Thin-Films. The charge-carrier mobility of the photoactive layer is an important factor dictating the performances of OPVs because it is directly related to the charge-transporting ability.[29] An OTFT with a bottom-contact geometry (channel length L = 12 μm and width W = 120 μm), using octadecyltrichlorosilane-treated SiO_2 and Au as the dielectric and source/drain electrodes, respectively, was fabricated using PTTBDT-FTT as the channel semiconductor. The device fabrication process is described in detail in the Experimental Section. Supporting Information Figure S5 shows the transfer curves for the polymers. The TFTs of the polymers were found to exhibit typical p-channel TFT characteristics. The TFT mobility was calculated in the saturation regime using the following equation:

$$I_{ds} = (WC_i/2L)\mu(V_{gs} - V_{th})^2$$

where I_{ds} is the drain/source current in the saturated region, W and L are the channel width and length, respectively, μ is the field-effect mobility, C_i is the capacitance per unit area of the insulating layer (SiO_2, 300 nm), and V_{gs} and V_{th} are the gate and threshold voltages, respectively.[30,31] The OTFTs fabricated using PTTBDT-FTT showed a hole mobility of 2.1 × 10^{-2} $cm^2/(V{\cdot}s)$ and on/off ratio of 10^5 (V_D = −60 V). It should be noted that this mobility value is comparable to, or exceeds, the value of the order of 10^{-3} $cm^2/(V{\cdot}s)$ that has been proposed to be necessary to reduce the photocurrent loss and obtain high-performance OPV devices.[32]

2.5. Regular Single-Layer BHJ OPV Performance and Film Morphology. In order to evaluate PTTBDT-FTT as a donor material for OPVs, BHJ OPVs were fabricated. Chlorobenzene containing 1,8-diiodooctane (DIO) as a processing additive was used to prepare solutions for spin-coating the active layers. Initially, different donor/acceptor (D/A) ratios [polymer/$PC_{71}BM$ (w/w), 1:1, 1:1.5, 1:2, and 1:3] were examined to find the optimum weight ratio. We found that the optimized conditions were a blend weight ratio of 1:1.5 and chlorobenzene containing 3 vol % DIO. The thickness of the active layers used in this work was ∼80 nm. DIO (3 vol %) was used as a processing additive. The current-density−voltage (J−V) characteristics of these OPVs were measured under AM 1.5G illumination (100 mW/cm^2) and are shown in Figure 3. The photovoltaic parameters of the fabricated OPVs are

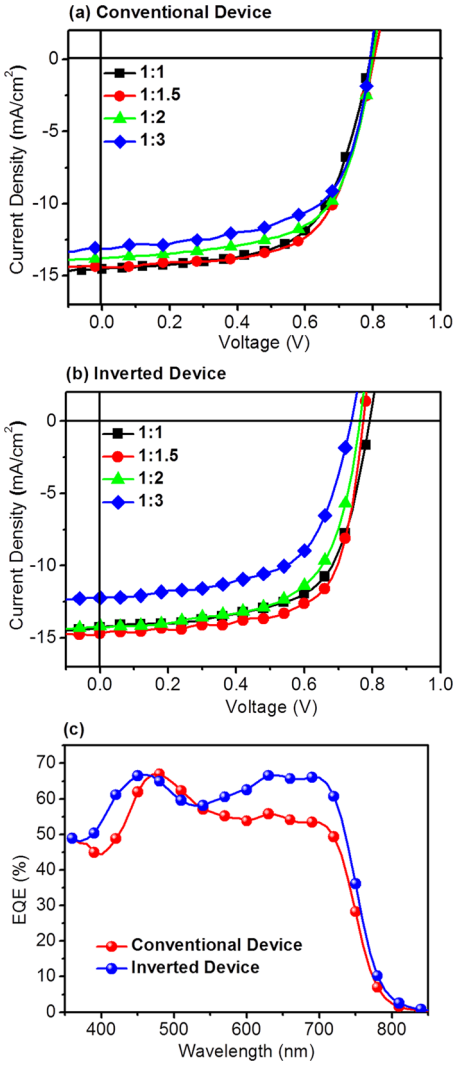

Figure 3. Current density−voltage (J−V) characteristics of the (a) conventional and (b) inverted OPV devices based on PTTBDT-FTT:$PC_{71}BM$ polymer blends with different ratios under illumination of AM 1.5G, 100 mW cm^{-2}. (c) EQEs of the corresponding devices.

summarized in Table 1. Conventional devices with the configuration ITO/PEDOT:PSS/PTTBDT-FTT:$PC_{71}BM$ (1:1.5, w/w)/Ca/Al exhibited a V_{oc} of 0.80 V, a J_{sc} of 14.40 mA/cm^2, and an FF of 0.64, delivering a PCE of 7.44%. Inverted cells with the configuration ITO/PEIE (ethoxylated polyethylenimine)/PTTBDT-FTT:$PC_{71}BM$ (1:1.5, w/w)/MoO_3/Ag were also fabricated, and the device showed a V_{oc} of 0.77 V, a J_{sc} of 14.70 mA/cm^2, and an FF of 0.68, delivering a high PCE of 7.71%. The improved efficiencies for the inverted devices are mainly a result of the increased J_{sc} and FF (14.70 versus 14.40 mA/cm^2 for the J_{sc} and 0.68 versus 0.64 for the FF).

The high J_{sc} is consistent with the broad absorption spectrum, high absorption coefficient, and high mobility of PTTBDT-FTT. The external quantum efficiency (EQE) curve in Figure 3c indicates that the PTTBDT-FTT:$PC_{71}BM$ active layer provides high photon-to-current conversion over a wide range of the visible spectrum region (350−800 nm).

Transmission electron microscopy (TEM) was used to obtain a real-space image of the phase-separated morphology of the polymer−fullerene blends. The TEM image is shown in

dx.doi.org/10.1021/cm4035903 | Chem. Mater. 2014, 26, 1234−1242

Table 1. Comparison of Photovoltaic Properties of OPVs Based on PTTBDT-FTT:$PC_{71}BM$ (Processed with 3 vol % DIO) with Different Weight Ratios, Measured under Illumination of AM 1.5 G, 100 mW/cm^2

cell type	ratio	V_{oc}[a] [V]	J_{sc}[a] [mA/cm^2]	FF[a]	PCE[a] [%]
conventional device[b]	1.0:1.0	0.78 ± 0.01	14.05 ± 0.5	0.62 ± 0.003	6.96 ± 0.18 (7.14)
	1.0:1.5	0.78 ± 0.02	14.20 ± 0.2	0.64 ± 0.002	7.09 ± 0.35 (7.44)
	1.0:2.0	0.79 ± 0.01	13.10 ± 0.7	0.63 ± 0.004	6.51 ± 0.46 (6.97)
	1.0:3.0	0.78 ± 0.01	12.84 ± 0.3	0.62 ± 0.005	6.36 ± 0.11 (6.47)
inverted device[c]	1.0:1.0	0.79 ± 0.01	14.29 ± 0.4	0.64 ± 0.002	6.96 ± 0.26 (7.22)
	1.0:1.5	0.76 ± 0.01	14.30 ± 0.4	0.68 ± 0.004	7.39 ± 0.32 (7.71)
	1.0:2.0	0.75 ± 0.01	13.89 ± 0.3	0.63 ± 0.003	6.56 ± 0.27 (6.83)
	1.0:3.0	0.73 ± 0.01	12.03 ± 0.2	0.61 ± 0.008	5.35 ± 0.13 (5.48)

[a]Photovoltaic properties of copolymers/$PC_{71}BM$-based devices spin-coated from a chloroform solution for polymers. Only the optimized recipes were considered for the estimation of the average PCE; data have been averaged over 10 devices. The performance of the best device is given in parentheses. [b]ITO/PEDOT:PSS/polymer:$PC_{71}BM$/Ca/Al configuration. [c]ITO/PEIE/polymer:$PC_{71}BM$/MoO_3/Ag configuration.

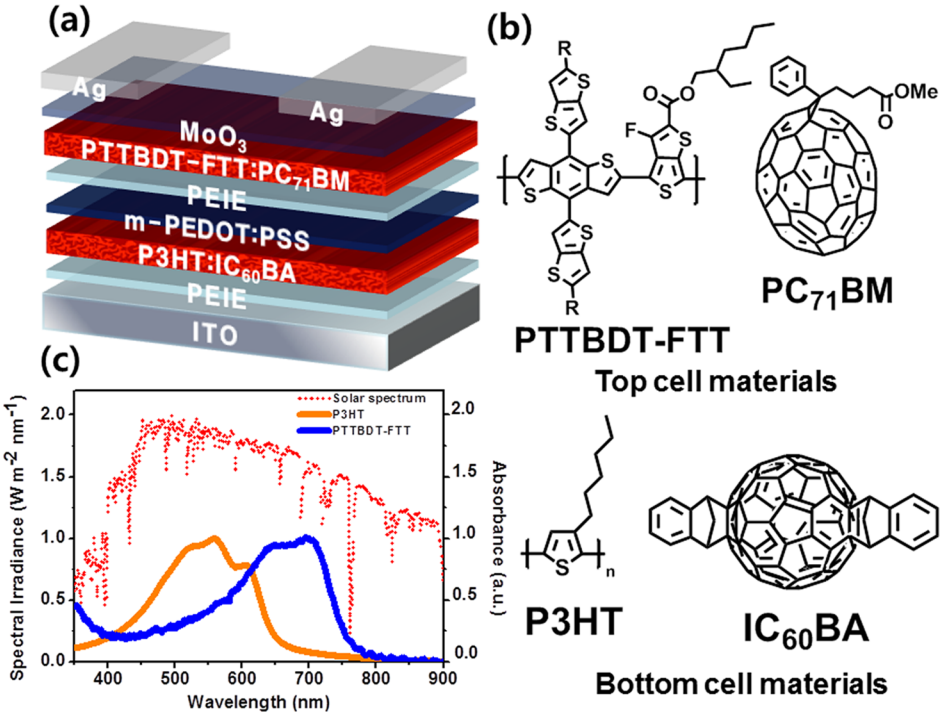

Figure 4. Inverted tandem photovoltaic device. (a) Device structure of the inverted tandem photovoltaic device. (b) Chemical structures of P3HT, $IC_{60}BA$, $PC_{71}BM$, and PTTBDT-FTT and (c) UV−visible spectra of the P3HT of bottom cell, the PTTBDT-FTT of top cell, and the solar spectrum.

Supporting Information Figure S6. The blend film revealed nanoscopically well-connected fibrous polymer domains. The intimately mixed and well-ordered domains within the matrix, together with the high hole mobility of the polymer, resulted in efficient charge separation and transport and, therefore, a high PCE.[33]

2.6. Inverted Tandem Photovoltaic Cell Performance. The high PCEs of the inverted photovoltaic cells encouraged us to fabricate tandem photovoltaic cells. Tandem OPVs, which consist of a bottom cell with a medium bandgap material, an interconnecting layer, and a top cell with a low bandgap material, effectively harvest a broader part of the solar spectrum and make more efficient use of the photonic energy than do single-junction structures.[34−37] Tandem OPVs with inverted configuration were fabricated using PTTBDT-FTT:$PC_{71}BM$ in the top cell and poly(3-hexylthiophene) (P3HT):indene-C_{60}-bisadduct ($IC_{60}BA$) in the bottom cell [ITO/PEIE/P3HT:$IC_{60}BA$ (150 nm)/PEDOT:PSS/PEIE/PTTBDT-FTT:$PC_{71}BM$ (80 nm)/MoO_3/Ag]. Figure 4 shows the device structure and the UV−visible absorption spectra of P3HT and PTTBDT-FTT in the solid state. The overlap of the absorption spectra of PTTBDT-FTT and P3HT is not significant, and the materials cover the solar spectrum from 350 to 800 nm complementarily, indicating a good match for the tandem structure. The tandem OPVs fabricated for this study have an inverted architecture with a conducting polymer layer of PEDOT:PSS, coated with PEIE as the charge recombination layer, as shown in Figure 4.[10,36] The $J-V$ characteristics of the tandem cells and the performance parameters are shown in Figure 5a. The optimized tandem cells exhibited maximum PCEs as high as 8.66%. The devices showed a V_{oc} of 1.57 V, which is equal to the sum of the V_{oc}'s of the single bottom and top cells; a J_{sc} of 8.31 mA/cm^2 and an FF higher than 0.66 were achieved.

Figure 6 shows the average photovoltaic parameters of the fabricated inverted tandem OPV devices. The 11 fabricated

dx.doi.org/10.1021/cm4035903 | Chem. Mater. 2014, 26, 1234−1242

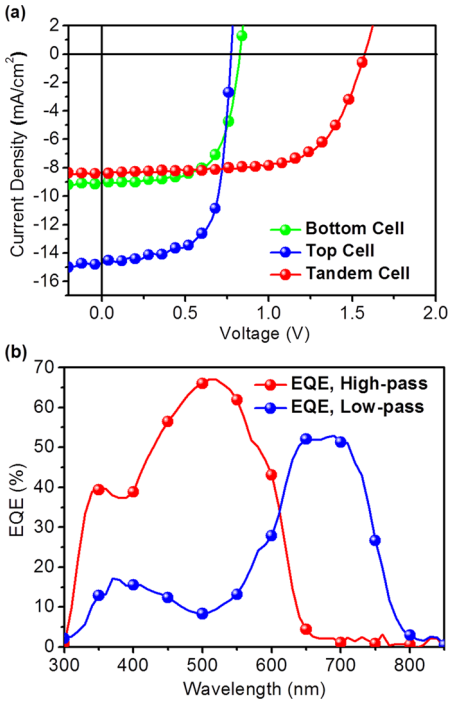

Figure 5. Current density−voltage characteristics of the single junction bottom cell, single junction top cell, and inverted tandem cell under AM 1.5G illumination (100 mW/cm^2). EQE of the P3HT:IC$_{60}$BA based bottom cell, PTTBDT-FTT:PC$_{71}$BM based top cell in a typical tandem device.

devices exhibited, on average, a PCE of 8.42%, a J_{sc} of 8.31 mA/cm^2, a V_{oc} of 1.57 V, and an FF of 0.66 (Supporting Information Table S2). To further confirm the J_{sc} achieved here, the EQEs of the two subcells in the tandem device were measured, using the reported method. As shown in Figure 5b, the bottom cell, which has a photoresponse from 300 to 650 nm, showed an EQE as high as 64% at 530 nm, and its integrated J_{sc} was 8.22 mA/cm^2. The top cell had a broad photoresponse from 300 to 800 nm, showed a maximum EQE of 52% at 710 nm, and its integrated J_{sc} was 7.07 mA/cm^2. These values are slightly lower than the device J_{sc}, which was attributed to some dimensional mismatch between the cell area (3 mm × 3 mm) and the beam size of the light source (1 mm × 4 mm) for EQE measurements despite our best effort to fit the beam into the largest active area of the cell. The photovoltaic performances of the inverted tandem devices are summarized in Table 2.

3. CONCLUSIONS

A new thieno[3,2-*b*]thiophene-substituted BDT derivative of 2,6-bis(trimethyltin)-4,8-bis((2-ethylhexyl)thieno[3,2-*b*]-thiophene)-benzo[1,2-*b*:4,5-*b*′]dithiophene was synthesized as a new donor building block for constructing donor−acceptor-type low bandgap polymers and was copolymerized with 2-ethylhexyl 4,6-dibromo-3-fluorothieno[3,4-*b*]thiophene-2-carboxylate to give PTTBDT-FTT. PTTBDT-FTT exhibited broad absorption, high molecular ordering with a predominantly face-on direction, and high hole mobility. The conventional single-cell device fabricated using a PTTBDT-FTT/PC$_{71}$BM blend exhibited a maximum PCE of 7.44%. The inverted device had enhanced J_{sc} and FF values, resulting in a PCE of 7.71%. Moreover, the tandem OPVs fabricated using PTTBDT-FTT:PC$_{71}$BM as the top cell and P3HT:IC$_{60}$BA as the bottom cell showed maximum PCEs of 8.66%.

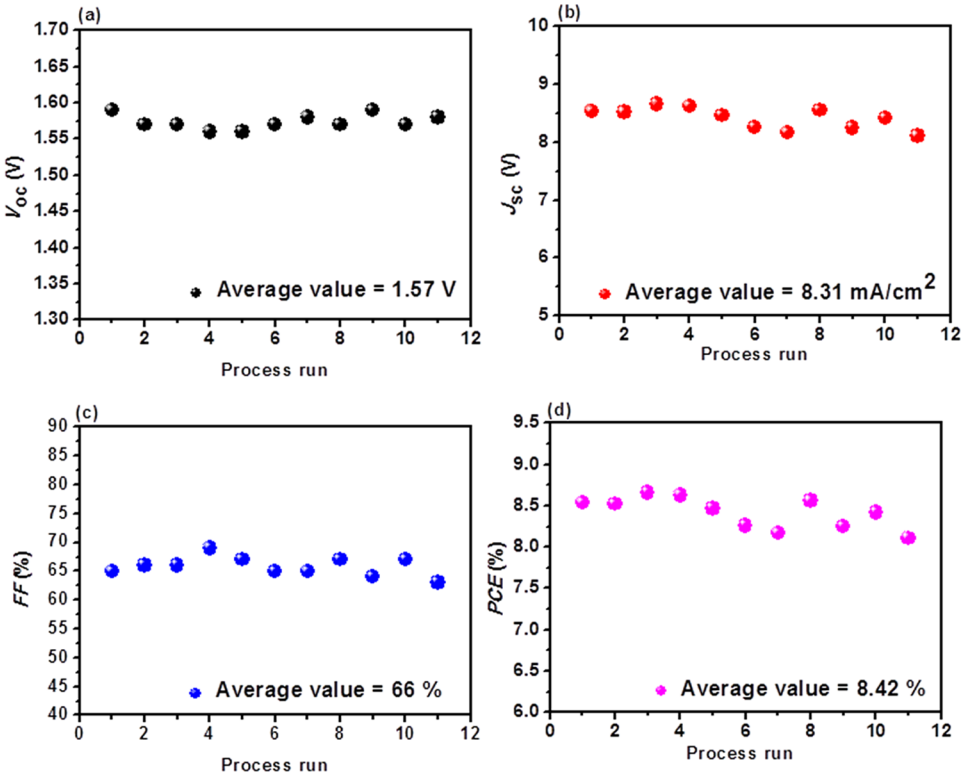

Figure 6. Photovoltaic parameters of the inverted tandem photovoltaic devices under AM 1.5G solar illumination; (a) open-circuit voltage, (b) short-circuit current density, (c) fill factor, and (d) power conversion efficiency as a function of average values.

dx.doi.org/10.1021/cm4035903 | *Chem. Mater.* 2014, 26, 1234−1242

Table 2. Characteristics of PTTBDT-FTT-Based Inverted Tandem OPVs (Inverted Single and Inverted Tandem) under Illumination of AM 1.5G, 100 mW/cm^2

	cell	active layer	ratio	thickness [nm]	V_{oc}[a] [V]	J_{sc}[a] [mA/cm^2]	FF[a]	PCE[a] [%]
inverted tandem cells	top cell[b]	PTTBDT-FTT:$PC_{71}BM$	1.0:1.5	80	0.77	14.70	0.68	7.71
	bottom cell[c]	P3HT:$IC_{60}BA$	1.0:1.0	150	0.83	9.03	0.66	4.93
	tandem cell[d]	-	-	-	1.57 ± 0.01	8.31 ± 0.56	0.66 ± 0.01	8.41 ± 0.19 (8.66)

[a]Photovoltaic properties of PTTBDT-FTT:$PC_{71}BM$-based devices spin-coated from a chlorobenzene solution for polymers. Only the optimized recipes were considered for the estimation of the average PCE; data have been averaged 10 devices. The performance of the best device is given in parentheses. [b]ITO/PEIE/PTTBDT-FTT:$PC_{71}BM$/MoO_3/Ag configuration. [c]ITO/PEIE/P3HT:$IC_{60}BA$/MoO_3/Ag configuration. [d]ITO/PEIE/P3HT:$IC_{60}BA$/PEDOT:PSS/PEIE/PTTBDT-FTT:$PC_{71}BM$/MoO_3/Ag configuration.

4. EXPERIMENTAL SECTION

4.1. Materials. Reagents were purchased from Aldrich, Alfa Aesar, or TCI Korea and used without further purification. [6,6]-Phenyl C_{71}-butyric acid methyl ester ($PC_{71}BM$) was purchased from EM-index. Solvents were dried and purified by fractional distillation over sodium/benzophenone and handled in a moisture-free atmosphere. Column chromatography was performed using silica gel (Merck, Kieselgel 60 63-200 MYM SC). 2-Ethylhexyl 4,6-dibromo-3-fluorothieno[3,4-*b*]thiophene-2-carboxylate (TT) was synthesized similarly to methods described in previous reports.[20−22]

4.2. Measurements. ^{1}H and ^{13}C NMR spectra were recorded using a Varian Mercury Plus 300 MHz spectrometer, and the chemical shifts were recorded in units of parts per million, with chloroform as an internal standard (δ 7.26 ppm). Elemental analysis was performed using a Vario Micro Cube at the Korea Basic Science Institute (Busan, Korea). Absorption spectra were obtained using a JASCO JP/V-570 spectrometer. The molecular weights of the polymers were determined via GPC analysis relative to a polystyrene standard using a Waters high-pressure GPC assembly (model M590). Thermal analyses were performed using a Mettler Toledo TGA/SDTA 851^e under a N_2 atmosphere, with heating and cooling rates of 10 °C/min. CV was performed using a CH Instruments Electrochemical Analyzer, to investigate the redox behavior of the polymers and determine their HOMO and LUMO energy levels. CV was carried out under an Ar atmosphere at room temperature in a solution of $TBABF_4$ (0.10 M) in acetonitrile at a scan rate of 50 mV/s. A Pt plate, Pt wire, and Ag/$AgNO_3$ electrode were used as the working, counter, and reference electrodes, respectively.

4.3. Two-Dimensional Grazing-Incidence X-ray Scattering (2D-GIXS) Experiments. 2D-GIXS measurements were performed using the beamline 3C-1 at the Pohang Accelerator Laboratory (South Korea). X-rays of wavelength 1.1651 Å (10.6408 keV) were used. The incidence angle (0.13°) was chosen to allow complete penetration of the X-rays into the polymer film. A thin layer (40−50 nm) of PEDOT:PSS was spin-coated onto Si substrates, and the polymer thin films were subsequently spin-coated on top.

4.4. Fabrication of OTFT Devices. OTFTs were fabricated using a bottom-contact geometry (channel length, L, 12 μm and width, W, 120 μm). The source and drain contacts were composed of Au (100 nm), and the dielectric comprised a 300 nm thick layer of SiO_2. The SiO_2 surface was cleaned, dried, and pretreated with a solution of 10.0 mM octyltrichlorosilane in toluene at room temperature for 2 h under a N_2 atmosphere to produce smooth, nonpolar surfaces, onto which the polymers were spin-coated. The polymers were dissolved in chlorobenzene at a concentration of 0.5 wt %. Films of the organic semiconductors were spin-coated at 1000 rpm for 50 s to form 60 nm thick layers. All device fabrication procedures and measurements were carried out in air at room temperature. The resultant TFTs exhibited typical p-channel TFT characteristics. The TFT mobilities were calculated in the saturation region, using the following equation:

$$I_{ds} = (WC_i/2L)\mu(V_G - V_T)^2$$

where I_{ds} is the drain/source current in the saturated region, W and L are the channel width (120 μm) and length (12 μm), respectively, μ is the field-effect mobility, C_i is the capacitance per unit area of the insulating layer (SiO_2, 300 nm), and V_G and V_T are the gate and threshold voltages, respectively.

4.5. Fabrication of Conventional Photovoltaic Devices. BHJ OPV devices with ITO/PEDOT:PSS/polymer:$PC_{71}BM$/Ca/Al structures were fabricated. The ITO surface was cleaned by sonication and rinsing in distilled water, methanol, and acetone. The hole-transporting PEDOT:PSS layer (45 nm) was spin-coated onto each ITO anode from a solution purchased from Heraeus (Clevios P VP AI4083), followed by spin-coating of a layer of polymer:$PC_{71}BM$; the polymer solution for spin-coating was prepared by dissolving the polymer (10 mg/mL) in a 97% chlorobenzene/3% DIO mixture. Ca and Al contacts were formed by vacuum deposition at pressures below 3×10^{-6} Torr, providing an active area of 0.09 cm^2.

4.6. Fabrication of Inverted Photovoltaic Devices. Inverted BHJ OPV devices with ITO/PEIE/polymer:$PC_{71}BM$/MoO_3/Ag structures were fabricated. The precleaned ITO substrates were treated with UV−ozone. The PEIE solution was spin coated onto ITO substrates at a speed of 5000 rpm for 1 min, with an acceleration of 1000 rpm/s, and annealed at 120 °C for 10 min on a hot plate in ambient air. The PEIE thickness was estimated to be 10 nm. The substrates were then transferred to a N_2-filled glovebox. The active layer of polymer:$PC_{71}BM$ (97% chlorobenzene/3% DIO mixture) was prepared by spin coating at a speed of 1000 rpm for 30 s. The device was solvent annealed for 1 h at ambient temperature in the glovebox. The device fabrication was completed by thermal evaporation of 10 nm MoO_3 and 100 nm Ag as the anode under vacuum at a base pressure of 3×10^{-6} Torr. The measured effective area of the device was 0.09 cm^2.

4.7. Fabrication of Inverted Tandem Cells. The device architecture of the tandem photovoltaic cell is shown in Figure 4. The precleaned ITO substrates were treated with UV−ozone. The PEIE solution was spin coated onto ITO the substrates at a speed of 5000 rpm for 1 min, with an acceleration of 1000 rpm/s, and annealed at 120 °C for 10 min on a hot plate in ambient air. The PEIE thickness was estimated to be 10 nm. The substrates were then transferred to a N_2-filled glovebox. The bottom layer of P3HT:$IC_{60}BA$ (1.0:1.0 weight ratio in *o*-dichlorobenzene) was prepared by spin coating at a speed of 800 rpm for 30 s. P3HT was purchased from Rieke Metals. $IC_{60}BA$ was purchased from EM-index. The P3HT:$IC_{60}BA$ device was solvent annealed for 1 h at ambient temperature in the glovebox. The hydrophilic PEDOT:PSS was directly coated onto the hydrophobic active layer by spin-casting a PEDOT:PSS layer of thickness 30 nm from Clevios P VP AI4083; the surfactant triton X-100 (1 wt %; laboratory grade; Sigma-Aldrich) was added to the aqueous solution of PEDOT:PSS. The PEDOT:PSS was then coated with PEIE, using the previously described conditions. The top active layer of PTTBDT-FTT:$PC_{71}BM$ (1:1.5 weight ratio in chlorobenzene with 3 vol % DIO) was deposited by spin-coating at 1000 rpm for 20 s. The PTTBDT-FTT:$PC_{71}BM$ thickness was estimated to be 80 nm. The device fabrication was completed by thermal evaporation of 10 nm MoO_3 and 100 nm Ag layers as the anode under vacuum at a base pressure of 3×10^{-6} Torr. The measured effective area of the device was 0.09 cm^2.

4.8. Measurement of OPV Devices. The thickness of the active layer was measured using a KLA Tencor Alpha-step IQ surface profilometer. The $J-V$ characteristics of the polymer photovoltaic cells were determined by illuminating the cells with simulated solar light

(AM 1.5G) at an intensity of 100 mW/cm^2 using an Oriel 1000 W solar simulator. Electronic data were recorded using a Keithley 236 Source-Measure Unit, and all characterizations were carried out under ambient conditions. The illumination intensity was calibrated using a standard Si photodiode detector from PV Measurements Inc.; it was calibrated at the National Renewable Energy Laboratory. The EQEs of the conventional and inverted single cells were measured as a function of wavelength in the range 360−900 nm using a 100 W halogen lamp outfitted with a monochromator and optical chopper; the photocurrent was measured using a lock-in amplifier, and the absolute photon flux was determined using a calibrated silicon photodiode. All device fabrication procedures and measurements were carried out in air at room temperature. The beam size of the light source was 3 mm × 3 mm. The EQE spectra of the tandem cells were measured using an incident photon-to-current conversion equipment (PV measurement Inc.). Calibration was performed using a silicon photodiode G425, which is NIST-calibrated as a standard at Korea Institute of Science and Technology (KIST). The EQE was selectively extracted from each subcell in the tandem device using a visible white-light-emitting diode (Daejin DMP Co.) with a light intensity of about 19 mW/cm^2 as bias lights. The wavelength of the bias light was controlled with optical filters (Andover Corporation). The EQEs of the bottom subcell and the top subcell in the tandem device were obtained using 550 nm high-pass and low-pass optical filters, respectively. The beam size of the light source was 4 mm ×1 mm.

4.9. Synthesis of Monomers and Polymers. *Synthesis of 2-(2-Ethylhexyl)thieno[3,2-b]thiophene (1).* Thieno[3,2-*b*]thiophene (10 g, 7.13 mmol) was dissolved in dry THF (100 mL) under a N_2 atmosphere; the solution was cooled to −78 °C and *n*-butyllithium (35 mL, 10.69 mmol, 2.0 M in hexane) was added dropwise. The reaction mixture was stirred at −78 °C for 1 h and then brought to room temperature. Stirring was continued for 20 min, and then the reaction mixture was cooled to −78 °C again. A solution of 2-ethylhexylbromide (12.7 mL, 10.69 mmol) was added dropwise. The mixture was slowly brought to room temperature and stirred overnight. Water was added to the reaction mixture, and the aqueous phase was extracted three times with ethyl acetate. The organic layer was separated and dried with anhydrous $MgSO_4$, and the resulting solution was concentrated by evaporation. The crude product was purified using silica column chromatography to give **1** as colorless oil (13.8 g, 80% yield). ^{1}H NMR (300 MHz, $CDCl_3$, ppm): δ 7.40 (d, 1H), 7.28 (d, 1H), 6.94 (s, 1H), 2.82 (d, 2H), 1.70 (m, 1H), 1.39 (m, 8H), 0.94 (m, 6H). ^{13}C NMR (75 MHz, $CDCl_3$, ppm): δ 141.8, 128.9, 125.4, 119.1, 118.5, 117.2, 48.3, 36.1, 33.8, 30.8, 27.5, 24.4, 15.4, 12.1.

Synthesis of 4,8-Bis((2-ethylhexyl)thieno[3,2-b]thiophene)-benzo[1,2-b:4,5-b′]dithiophene (2). Compound **1** (4.5 g, 1.80 mmol) and THF (100 mL) were added to a flask under an inert atmosphere. The solution was cooled using an ice−water bath, and 9.2 mL of *n*-butyllithium (2.67 mmol, 2.0 M in pentane) was added dropwise to the flask. The mixture was warmed to 50 °C and stirred for 2 h. 4,8-Dehydrobenzo[1,2-*b*:4,5-*b*′]dithiophene-4,8-dione (1.00 g, 0.45 mmol) in THF (20 mL) was added, and the mixture was stirred for 1 h at 50 °C. After cooling to ambient temperature, $SnCl_2{\cdot}2H_2O$ (8.00 g, 14.4 mmol) in 10% HCl (16 mL) was added, and the mixture was stirred for an additional 2 h. The resulting solution was poured into 200 mL of methanol and extracted three times with ethyl acetate. The organic layer was separated and dried with anhydrous $MgSO_4$. The obtained crude product was purified using silica-gel column chromatography, with methylene chloride/hexane as the eluent. A yellow solid was obtained after removing the solvents (3.0 g, 75% yield). ^{1}H NMR (300 MHz, $CDCl_3$, ppm): δ 7.68 (d, 2H), 7.57 (s, 2H), 7.50 (d, 2H), 7.02 (s, 2H), 2.89 (d, 4H), 1.88 (m, 2H), 1.59−1.28 (m, 16H), 0.94−0.88 (m, 12H). ^{13}C NMR (75 MHz, $CDCl_3$, ppm): δ 145.5, 139.1, 134.1, 133.9, 132.1, 128.7, 126.1, 125.0, 124.2, 122.5, 120.1, 49.1, 42.5, 39.3, 35.8, 28.4, 27.1, 16.4, 12.7. Anal. Calcd for $C_{38}H_{42}S_6$: C, 66.04; H, 6.13; S, 27.84. Found: C, 65.98; H, 6.10; S, 27.70.

Synthesis of 2,6-Bis(trimethyltin)-4,8-bis((2-ethylhexyl)thieno[3,2-b]thiophene)-benzo[1,2-b:4,5-b′]dithiophene (TTBDT). Compound **2** (1.2 g, 0.17 mmol), *N*,*N*,*N*′,*N*′-tetramethylethylenediamine (0.7 mL, 0.43 mmol), and THF (100 mL) were added to a flask under an inert atmosphere. The solution was cooled to −78 °C, and 1.8 mL of *n*-butyllithium (3.00 mL, 0.43 mmol, 2.0 M in pentane) were added. The solution was stirred at −78 °C for 1 h and then 4.3 mL of trimethyltin chloride (0.43 mmol, 1.0 M in THF) was added in one portion. The reaction mixture was stirred for 2 h, and the cooling bath was then removed. The reaction mixture was heated to room temperature and stirred for 12 h. The resulting solution was poured into 200 mL of cold water and extracted three times with ethyl acetate. The organic layer was separated and dried with anhydrous $MgSO_4$. The solvent was removed under vacuum, and then the residue was crystallized in methanol. A yellow solid was obtained (1.1 g, 75% yield). ^{1}H NMR (300 MHz, $CDCl_3$, ppm): δ 7.78 (s, 2H), 7.60 (s, 2H), 7.02 (s, 2H), 2.95 (d, 4H), 1.88 (m, 2H), 1.59−1.28 (m, 16H), 0.94−0.88 (m, 12H), 0.38 (s, 18H). ^{13}C NMR (75 MHz, $CDCl_3$, ppm): δ 144.1, 140.9, 138.2, 135.7, 134.2, 130.5, 128.0, 125.4, 123.1, 119.6, 119.1, 48.7, 45.1, 40.3, 32.1, 30.7, 26.4, 22.9, 14.4, −144. Anal. Calcd for $C_{44}H_{58}S_6Sn_2$: C, 51.98; H, 5.75; S, 18.92. Found: C, 51.80; H, 5.71; S, 18.88.

Poly{4,8-bis((2-ethylhexyl)thieno[3,2-b]thiophene)-benzo[1,2-b:4,5-b′]dithiophene-alt-2-ethylhexyl-4,6-dibromo-3-fluorothieno-[3,4-b]thiophene-2-carboxylate} (PTTBDT-FTT). The Stille cross-coupling reaction was used to synthesize the copolymers. TTBDT (400 mg, 0.40 mmol) was mixed with FTT (195 mg, 0.40 mmol, 1.0 equiv), $Pd(PPh_3)_4$ (15.2 mg, 2.6 μmol), toluene (12 mL), and DMF (3 mL) for the polymerization. The reaction mixture was stirred at 110 °C for 2 d, then excess 2-bromothiophene and tripropyl(thiophen-2-yl)stannane, the end-capper, dissolved in 1 mL of anhydrous toluene, was added, and stirring was continued for 12 h. For polymer purification, the reaction mixture was cooled to approximately 50 °C, and 200 mL of methanol was added slowly with vigorous stirring of the reaction mixture. The polymer fibers were collected by filtration and reprecipitation from methanol and acetone. The polymer was then further purified by washing for 2 d in a Soxhlet apparatus with acetone to remove oligomers and catalyst residues. Column chromatography using a chloroform solution was then performed on the polymer. The reprecipitation procedure in chloroform/methanol was repeated several times. The polymer yield was 48%. The resulting polymers were soluble in common organic solvents. ^{1}H NMR (300 MHz, $CDCl_3$, ppm) δ: 8.05−7.90 (br, 2H), 7.65−7.08 (br, 4H), 3.51−3.30 (br, 1H), 3.05−2.78 (br, 4H), 2.64−0.61 (br, 44H).

■ ASSOCIATED CONTENT

Supporting Information

TGA and DSC measurements of the polymer, GPC traces, OTFT performance of the polymer, TEM image, and the additional data. This material is available free of charge via the Internet at http://pubs.acs.org

■ AUTHOR INFORMATION

Corresponding Author

*E-mail: dohoonhwang@pusan.ac.kr.

Notes

The authors declare no competing financial interest.

■ ACKNOWLEDGMENTS

This work was supported by a grant (No. 2012055225) from the Center for Advanced Soft Electronics under the Global Frontier Research Program of the Ministry of Education, Science and Technology, a New and Renewable Energy Program of the Korea Institute of Energy Technology Evaluation and Planning (KETEP), funded by the Ministry of Knowledge Economy (MKE) (20113010010030), and an NRF grant funded by the Korean Government (NRF-2013-Global Ph.D. Fellowship Program).

■ ABBREVIATIONS

BDT, benzodithiophene; BDTT, benzo[1,2-*b*:4,5-*b*′]-dithiophenes; BHJ, bulk heterojunction; CV, cyclic voltammetry; D/A, donor/acceptor; DIO, 1,8-diiodooctane; EQE, external quantum efficiency; FF, fill factor; FTT, 2-ethylhexyl 3-fluorothieno[3,4-*b*]thiophene-2-carboxylate; GPC, gel permeation chromatography; HOMO, highest occupied molecular orbital; $IC_{60}BA$, indene-C_{60}-bisadduct; J_{sc}, short-circuit currents; *J*−*V*, current-density−voltage; LUMO, lowest unoccupied molecular orbital; M_n, number-average molecular-weight; OPV, organic photovoltaic cell; OTFT, organic thin-film transistor; $PC_{71}BM$, [6,6]-phenyl C_{71}-butyric acid methyl ester; PCE, power conversion efficiency; PDI, polydispersity index; PEIE, ethoxylated polyethylenimine; P3HT, poly(3-hexylthiophene); PTB7, poly({4,8-bis[(2-ethylhexyl)oxy]-benzo[1,2-*b*:4,5-*b*′]dithiophene-2,6-diyl}-*alt*-{3-fluoro-2-[(2-ethylhexyl)carbonyl]thieno[3,4-*b*]thiophenediyl}); PTTBDT-FTT, poly{4,8-bis((2-ethylhexyl)thieno[3,2-*b*]thiophene)-benzo[1,2-*b*:4,5-*b*′]dithiophene-*alt*-2-ethylhexyl-4,6-dibromo-3-fluorothieno[3,4-*b*]thiophene-2-carboxylate}; $TBABF_4$, tetrabutylammonium tetrafluoroborate; TEM, transmission electron microscopy; TGA, thermogravimetric analysis; TT, thiophene-2-carboxylate; TT, thieno[3,4-*b*]thiophene; TTBDT, bis(2-ethylhexylthieno[3,2-*b*]thiophenylbenzo[1,2-*b*:4,5-*b*′]-dithiophene; V_{oc}, open-circuit voltages

■ REFERENCES

(1) Park, S. H; Roy, A.; Beaupre, S.; Cho, S.; Coates, N.; Moon, J. S; Moses, D.; Leclerc, M.; Lee, K.; Heeger, A. J. *Nat. Photonics* **2009**, *3*, 297−302.

(2) Sariciftci, N. S.; Smilowitz, L.; Heeger, A. J.; Wudl, F. *Science* **1992**, *258*, 1474−1476.

(3) Xin, H.; Subramaniyan, S.; Kwon, T.-W.; Shoaee, S.; Durrant, J. R.; Jenekhe, S. A. *Chem. Mater.* **2012**, *24*, 1995−2001.

(4) Krebs, F. C.; Gevorgyan, S. A.; Alstrup, J. *J. Mater. Chem.* **2009**, *19*, 5442−5451.

(5) Helgesen, M.; Søndergaard, R.; Krebs, F. C. *J. Mater. Chem.* **2010**, *20*, 36−60.

(6) Park, J. K.; Jo, J.; Seo, J. H.; Moon, J. S.; Park, Y. D.; Lee, K.; Heeger, A. J.; Bazan, G. C. *Adv. Mater.* **2011**, *23*, 2430−2435.

(7) Sista, S.; Hong, Z.; Chen, L. M.; Yang, Y. *Energy Environ. Sci.* **2011**, *4*, 1606−1620.

(8) Ameri, T.; Dennler, G.; Lungenschmied, C.; Brabec, C. J. *Energy Environ. Sci.* **2009**, *2*, 347−363.

(9) Kim, J. Y.; Lee, K.; Coates, N. E.; Moses, D.; Nguyen, T. Q.; Dante, M.; Heeger, A. J. *Science* **2007**, *317*, 222−225.

(10) Zhou, Y. H.; Fuentes-Hernandez, C.; Shim, J. W.; Khan, T. M.; Kippelen, B. *Energy Environ. Sci.* **2012**, *5*, 9827−9832.

(11) Gevaerts, V. S.; Furlan, A.; Wienk, M. M.; Turbiez, M.; Janssen, R. A. J. *Adv. Mater.* **2012**, *24*, 2130−2134.

(12) Li, W.; Furlan, A.; Hendriks, K. H.; Wienk, M. M.; Janssen, R. A. J. *J. Am. Chem. Soc.* **2013**, *135*, 5529−5532.

(13) Dennler, G.; Scharber, M. C.; Ameri, T.; Denk, P.; Forberich, K.; Waldauf, C.; Brabec, C. J. *Adv. Mater.* **2008**, *20*, 579−583.

(14) Heliatek website. http://www.heliatek.com (accessed June 2013).

(15) Dou, L.; Chang, W.-H.; Gao, J.; Chen, C.-C.; You, J.; Yang, Y. *Adv. Mater.* **2013**, *25*, 825−831.

(16) You, J.; Dou, L.; Yoshimura, K.; Kato, T.; Ohya, K.; Moriarty, T.; Emery, K.; Chen, C. C.; Gao, J.; Li, G.; Yang, Y. *Nat. Commun.* **2013**, *4*, 1446−1455.

(17) Huo, L.; Hou, J.; Zhang, S.; Chen, H.-Y.; Yang, Y. *Angew. Chem., Int. Ed.* **2010**, *49*, 1500−1503.

(18) Zhang, M.; Gu, Y.; Guo, X.; Liu, F.; Zhang, S.; Huo, L.; Russell, T. P.; Hou, J. *Adv. Mater.* **2013**, *25*, 4944−4949.

(19) Hou, J.; Chen, H.-Y.; Zhang, S.; Chen, R. I.; Yang, Y.; Wu, Y.; Li, G. *J. Am. Chem. Soc.* **2009**, *131*, 15586−15587.

(20) Huo, L. J.; Zhang, S. Q.; Guo, X.; Xu, F.; Li, Y. F.; Hou, J. H. *Angew. Chem., Int. Ed.* **2011**, *50*, 9697−9702.

(21) Chen, H. Y.; Hou, J. H.; Zhang, S. Q.; Liang, Y. Y.; Yang, G. W.; Yang, Y.; Yu, L. P.; Wu, Y.; Li, G. *Nat. Photonics* **2009**, *3*, 649−653.

(22) Price, S. C.; Stuart, A. C.; Yang, L.; Zhou, H.; You, W. *J. Am. Chem. Soc.* **2011**, *133*, 4625−4631.

(23) Liao, S.-H.; Jhuo, H.-J.; Cheng, Y.-S.; Chen, S.-A. *Adv. Mater.* **2013**, *25*, 4766−4771.

(24) Huang, Y.; Guo, X.; Liu, F.; Huo, L.; Chen, Y.; Russell, T. P.; Han, C. C.; Li, Y.; Hou, J. *Adv. Mater.* **2012**, *24*, 3383−3389.

(25) Lee, D.; Hubijar, E.; Kalaw, G. J. D.; Ferraris, J. P. *Chem. Mater.* **2012**, *24*, 2534−2540.

(26) Li, K.; Li, Z.; Feng, K.; Xu, X.; Wang, L.; Peng, Q. *J. Am. Chem. Soc.* **2013**, *135*, 13549−13557.

(27) Cho, H.-H.; Kang, T. E.; Kim, K.-H.; Kang, H.; Kim, H. J.; Kim, B. *Macromolecules* **2012**, *45*, 6415−6417.

(28) Kim, J.-H.; Song, C. E.; Shin, N.; Kang, H.; Wood, S.; Kang, I.-N.; Kim, B. J.; Kim, B. S.; Kim, J.-S.; Shin, W. S.; Hwang, D.-H. *ACS Appl. Mater. Interfaces* **2013**, *5*, 12820−12831.

(29) Ahmed, E.; Subramaniyan, S.; Kim, F. S.; Xin, H.; Jenekhe, S. A. *Macromolecules* **2011**, *44*, 7207−7219.

(30) Shaw, J. M.; Seidler, P. F. *IBM J. Res. Dev.* **2001**, *45*, 3−9.

(31) Dimitrakopoulos, C. D.; Mascaro, D. J. *IBM J. Res. Dev.* **2001**, *45*, 11−27.

(32) Coakley, K. M.; McGehee, M. D. *Chem. Mater.* **2004**, *16*, 4533−4542.

(33) Kim, J.-H.; Song, C. E.; Kang, I.-N.; Shin, W. S.; Hwang, D.−H. *Chem. Commun.* **2013**, *49*, 3248−3250.

(34) Hadipour, A.; de Boer, B.; Wildemann, J.; Kolstra, F. B.; Hummelen, J. C.; Turbiez, M. G. R.; Wienk, M. M.; Janssen, R. A. J.; Blom, P. W. M. *Adv. Funct. Mater.* **2006**, *16*, 1897−1903.

(35) Hadipour, A.; de Boer, B.; P. Blom, W. M. *Adv. Funct. Mater.* **2008**, *18*, 169−181.

(36) Zhou, Y. H.; Fuentes-Hernandez, C.; Shim, J.; Meyer, J.; Giordano, A. J.; Li, H.; Winget, P.; Papadopoulos, T.; Cheun, H.; Kim, J.; Fenoll, M.; Dindar, A.; Haske, W.; Najafabadi, E.; Khan, T. M.; Sojoudi, H.; Barlow, S.; Graham, S.; Brédas, J.-L.; Marder, S. R.; Kahn, A.; Kippelen, B. *Science* **2012**, *336*, 327−332.

(37) Kim, J.-H.; Song, C. E.; Kim, H. U.; Grimsdale, A. C.; Moon, S.-J.; Shin, W. S.; Choi, S. K.; Hwang, D.-H. *Chem. Mater.* **2013**, *25*, 2722−2732.